Research Article

Xin Jin*, Jifeng Zhang*, Cuilong Liu, Xuan Gao, Xiao Luo, Shiyao Qi, Zhenyang Yu, and Haotian Guo

Influence of stitching parameters on the tensile performance and failure mechanisms of CFRP T-joints

https://doi.org/10.1515/epoly-2025-0061
received August 11, 2025; accepted August 30, 2025

Abstract: T-joints made from carbon fiber reinforced polymer (CFRP) composites are widely used in aircraft fuselages. However, CFRP structures are prone to interlaminar delamination, for which stitching reinforcement presents a promising solution. Therefore, this work presents an experimental study on the tensile behavior of stitched T-joints, in which key stitching parameters (stitch method, fineness, and needle distance) are systematically investigated to assess their influence on mechanical performance and to elucidate the underlying reinforcement mechanisms. Stitching enhances the Mode I fracture toughness and tensile strength of T-joints, with the lock-stitch providing the superior improvement. However, an optimal stitch fineness (1,000D) exists, as excessive fineness degraded performance from its peak, while still outperforming the unstitched baseline. Reducing the needle distance results in a 27% increase in peak load, as stitching improves tensile strength by increasing constraint density and regulating crack propagation. Meanwhile, ductile fracture of the Kevlar fibers and stress bridging by the stitches are the two primary mechanisms driving the interlaminar toughness enhancement.

Keywords: CFRP, T-joints, stitch method, failure mechanism, mode I interlaminar fracture toughness

*** Corresponding author: Xin Jin,** College of Aerospace and Civil Engineering, Harbin Engineering University, Harbin, China, e-mail: hg368jx@163.com
*** Corresponding author: Jifeng Zhang,** College of Aerospace and Civil Engineering, Harbin Engineering University, Harbin, China, e-mail: jfzhang@hrbeu.edu.cn
Cuilong Liu, **Xuan Gao**, **Xiao Luo**, **Shiyao Qi**, **Zhenyang Yu:** School of Civil and Architecture Engineering, Jiangxi University of Water Resources and Electric Power, Nanchang, China
Haotian Guo: College of Aerospace and Civil Engineering, Harbin Engineering University, Harbin, China

1 Introduction

Carbon fiber reinforced polymers (CFRPs) have been widely applied in cutting-edge fields such as aerospace main load-bearing structures, new energy vehicles, and deep-sea equipment (1–3) due to their outstanding specific strength, high specific stiffness, lightweight properties (4), corrosion resistance, and high fatigue endurance (5–7). Composite T-joints are essential for load transfer between orthogonal components in major structures such as aircraft fuselages and wind turbine blades. However, the junction between the web and flange creates significant geometric discontinuity, leading to high stress concentrations that make this region a primary failure point (8). Specifically, out-of-plane loading induces severe interlaminar stresses, which, coupled with the inherent lack of through-thickness reinforcement in traditional laminates, frequently initiates catastrophic delamination failure (9–11).

This inherent structural vulnerability has spurred the development of various through-thickness reinforcement strategies. Macro-scale approaches create spatial interlocking structures through techniques such as stitching (12,13), Z-pin (14,15), or three-dimensional weaving technology (16–19). However, there are significant limitations of the prior art: Z-pin implantation leads to in-plane strength attenuation (20), and interface fretting wear causes stiffness degradation under high cycle fatigue (21). Furthermore, due to the high cost of equipment and the limited fiber volume fraction, 3D weaving technology is difficult to adapt to complex structures (22,23).

Compared to Z-pinning, stitching offers superior design flexibility and better preserves in-plane properties by providing localized reinforcement with minimal fiber disruption. As a mechanical reinforcement, stitching establishes robust crack-bridging mechanisms, offering a more direct and cost-effective solution than chemical modifications or 3D weaving. Characterizing the Mode I and Mode II interlaminar fracture toughness has become a standard approach for evaluating the efficacy of stitching as a through-thickness reinforcement

technique. Highlighting the critical role of the stitch material, Ravandi et al. (24) investigated natural fiber stitching and found that while flax yarn improved the Mode I interlaminar fracture toughness by at least 10%, cotton thread stitches provided no significant toughening benefit. Tapullima et al. (25) particularly focused on using cohesive zone model to simulate crack propagation and identify the stitch pattern and stitch head as critical factors influencing the reinforcement effect. Su et al. (26) showed that stitching processes can significantly improve the interlaminar properties of needle-punched/stitched multi-scale interlock composites. The main failure modes of double-notched shear in these composites are matrix cracking, brittle fracture of fiber bundles, and pull-out.

The influence of stitching on the tensile behavior and failure mechanisms of composite T-joints has been garnering increasing research attention. Kumari and Sinha (27) investigated how transverse stitch and damp heat environments can exacerbate the transverse and shear stresses at the web–skin interface of carbon fiber composite T-joints, making this region a critical area for failure. Zhang et al. (28) found that hail impact can cause delamination damage and reduce the tensile strength of composite T-joints, but stitch reinforcement can effectively inhibit delamination propagation and significantly improve the ultimate displacement and bearing capacity of the joints. Kim et al. (29) developed a novel single-thread stitching method that prevents carbon fiber breakage, yielding composite T-joints with superior strength compared to conventional Z-pinning. Investigating T-joints fabricated with one-side stitching and the RTM process, Bigaud et al. (30) utilized digital image correlation technology to optimize the stitching positions. This approach led to a 25% improvement in ultimate strength and a 19% increase in post-peak load recovery. Huan et al. (31) conducted tensile experiments to study the mechanism of stitch on the interface reinforcement of T-joints. The results show that both stitch density and stitch fineness had an effect on the tensile ultimate load of T-joints. While these studies offer valuable insights, they often lack a quantitative analysis of the effect of key stitching parameters on mechanical properties, as well as a comprehensive understanding of the associated mechanisms of crack initiation, propagation, and failure.

Therefore, this work presents a detailed experimental investigation into the tensile behavior and underlying reinforcement mechanisms of stitched T-joints, with a particular focus on key stitching parameters (stitch method, fineness, and needle distance). The structure of this study is as follows: Section 2 describes the materials and methods, covering specimen preparation, stitching parameters, and the test setup. Section 3 presents results and discussion on Mode I interlaminar fracture toughness and T-joint tensile tests. Finally, Section 4 summarizes the main conclusions of this work.

2 Experimental methods

2.1 Manufacture of stitched T-joint and tensile test

Each T-joint is stitched through the flange-skin interface on both sides of the web, with the stitch line positioned 10 mm from the web. Kevlar thread is employed to ensure better stitching effect. The web and two L-shaped stiffeners are each constructed from six plies of carbon fiber prepreg arranged in a $[0/90]_3$ stacking sequence. The reinforcement stitching involved three main variables: stitch method, fineness, and needle distance. As shown in Figure 1, four stitching methods are investigated, including improved lock stitch (LS), chain stitch (CS), flat stitch (FS), and temporary stitch (TS). The stitching is performed using threads of three different deniers (500D, 1,000D, and 1,500D) with three distinct needle distances (10, 15, and 20 mm).

Specimens are fabricated via a hot-press molding process as shown in Figure 2. Stitched carbon fiber prepreg

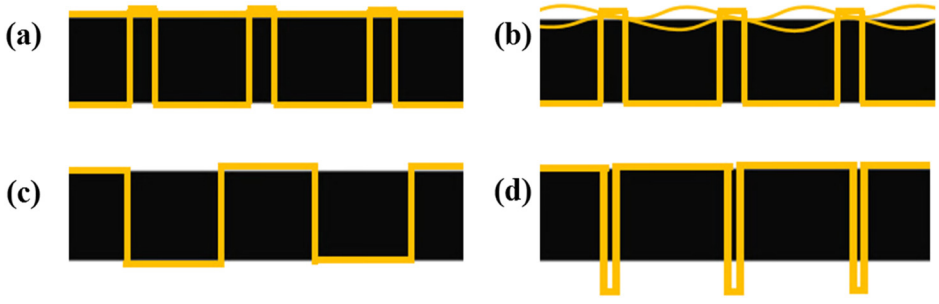

Figure 1: Diagram of the stitch method: (a) improved LS, (b) CS, (c) FS, and (d) TS.

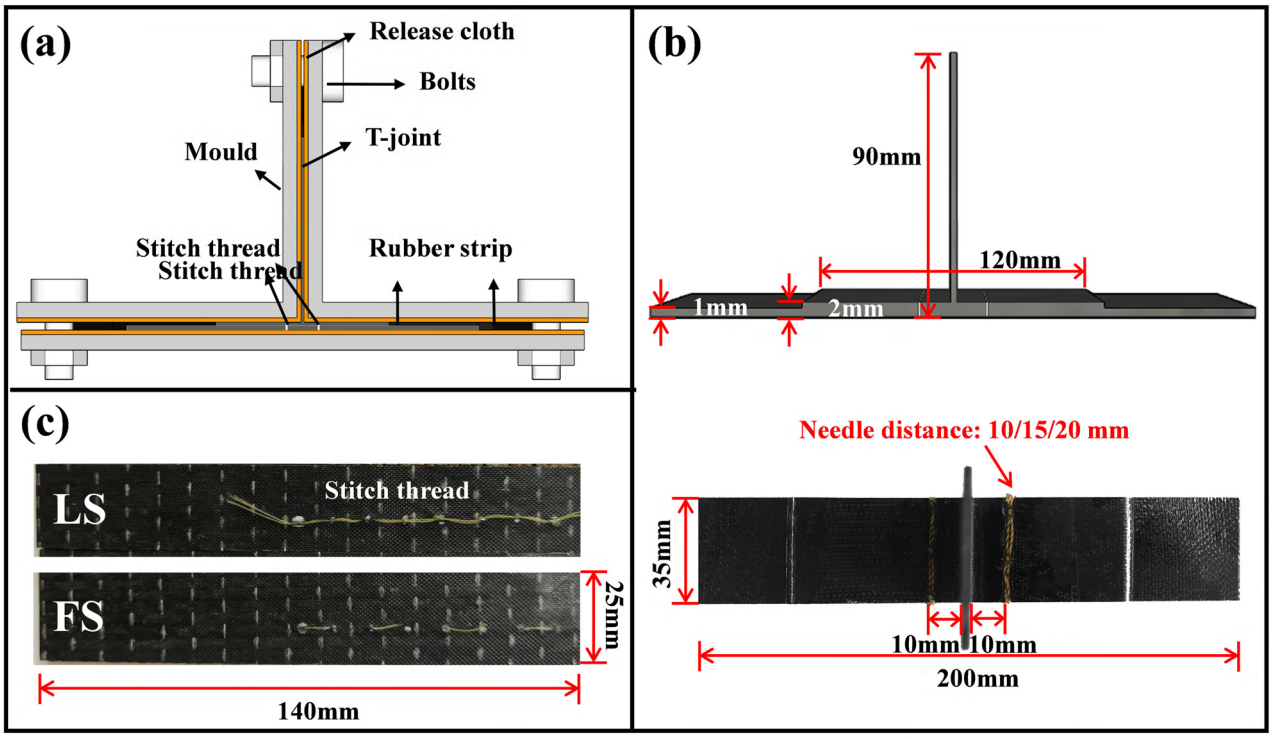

Figure 2: (a) Fabrication progress, (b) T-joints, and (c) specimens for Mode I interlaminar tests.

preforms are placed in a steel mold (a plate and two steel angles) lined with a release fabric, with bolts used for pressurization. Curing is performed in an oven at 150°C for 1 h, followed by natural cooling to ambient temperature before demolding. The fiber volume fraction of the specimen is 50%. The as-cured parts are then machined to the final dimensions of 200 mm × 35 mm × 90 mm ($L \times W \times H$) and a nominal thickness of 2 mm (Figure 2). The specific stitching parameters for each specimen configuration are listed in Table 1.

Table 1: Test matrix of T-joint tension

Specimen name	Stitch method	Stitch fineness (D)	Needle distance (mm)
NS	Not stitch	—	—
FS-500-10	FS	500	10
CS-500-10	CS	500	10
TS-500-10	TS	500	10
LS-500-10	Improve LS	500	10
LS-500-15	Improve LS	500	15
LS-500-20	Improve LS	500	20
LS-1000-10	Improve LS	1,000	10
LS-1000-15	Improve LS	1,000	15
LS-1000-20	Improve LS	1,000	20
LS-1500-10	Improve LS	1,500	10
LS-1500-15	Improve LS	1,500	15
LS-1500-20	Improve LS	1,500	20

The tensile test of T-joint is carried out by CSS-44100 universal testing machine, and the fixture is fixed to the machine through the protruding block at the lower part, and the specimen is fixed by four screws to prevent it from sliding as shown in Figure 3. All the tensile tests are conducted at a speed of 1 mm·min^{-1} at room temperature. During the tensile process, the deformation of T-joints is observed on the macroscopic scale with the help of a digital camera.

2.2 Specimen preparation and mode I interlaminar test

In Figure 2(c), all the double cantilever beam (DCB) coupons are prepared by hot-press molding, with $[0/90]_{6s}$ stacking sequence and nominal dimensions of 140 mm (l) × 25 mm (b) × 4 mm (h). An initial delamination of 52 mm in length is introduced by embedding a polyimide film at the mid-plane of one end.

To investigate the influence of various stitch methods on Mode I interlaminar fracture toughness, the tests are conducted by DCB specimens in accordance with the ASTM

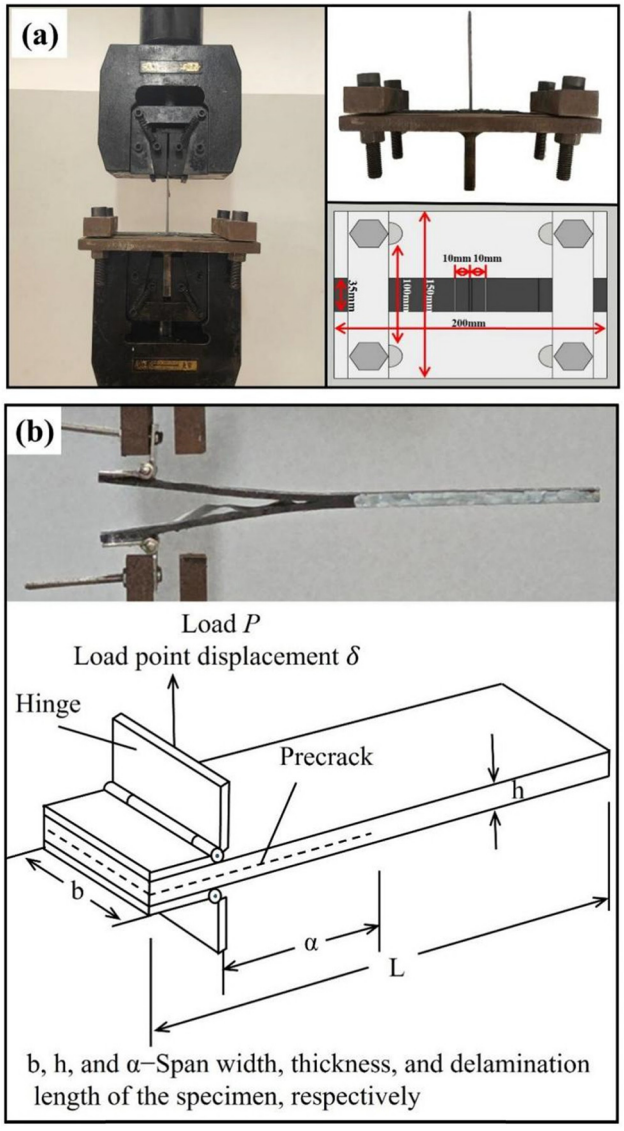

Figure 3: The experimental setup: (a) tensile test of T-joints and (b) Mode I interlaminar test.

D5528-13 standard (32). The experimental setup is illustrated in Figure 3(b). The test for fracture toughness is conducted on a universal testing machine at a test rate of 1 mm·min^{-1}. Each test is terminated once the crack has fully propagated through the specimen. To facilitate the observation of crack propagation, a scaled paper ruler is adhered to the side of specimen. Three replicate tests are performed for each configuration. The Mode I interlaminar fracture toughness of the laminates is calculated by using the Modified Beam Theory according to the following equation:

$$G_{\mathrm{I}} = \frac{3P\delta}{2b(a+\Delta)} \tag{1}$$

where G_{I} is the Mode I interlaminar fracture toughness, or strain energy release rate (J·m^{-2}); P is the applied load (N); δ is the load-point displacement (mm); b is the specimen width (mm); a is the effective crack length (mm); and Δ is the length of the crack at $P_{\max}$.

3 Results and discussion

3.1 Effect of stitch method on Mode I interlaminar fracture toughness tests

Investigations presented in Sections 3.1 and 3.2 were conducted on specimens fabricated with a standardized set of stitching parameters: a fineness of 500D and a pitch of 10 mm. This methodology was adopted to isolate the influence of various stitching patterns on the interlaminar toughness. Figure 4(a) displays the typical load–displacement curves for specimens with various stitching methods subjected to Mode I interlaminar fracture toughness tests. The curve trends are largely similar across different methods. Video recordings reveal crack initiation and propagation. The load reached its peak value as the crack front extended to the first stitch hole, which corresponds to a crack extension of approximately 5 mm. At this point, stitch failure occurred, leading to a subsequent drop in load. As the crack reached subsequent stitch holes, its growth was briefly arrested, producing slight load rises and two to three local peaks on the curve.

Figure 4(b) presents the G_{I} for all specimens, calculated using Eq. 1. All four stitching methods significantly enhanced the interlaminar fracture toughness. Notably, the LS method doubled the toughness, indicating that it is the most effective approach for improving the Mode I interlaminar performance. As observed in the morphologies of Figure 5, the interlaminar fracture surfaces of the unstitched and stitched specimens exhibit no significant differences, both showing rough areas characteristic of matrix/fiber debonding. This suggests that the enhancement in Mode I interlaminar fracture toughness is primarily attributed to the fracture of the stitches.

3.2 Effect of stitch method on tensile performance of T-joints

In Figure 6, it is worth noting that the curve is divided into three stages: first, the specimen is in the linear elastic

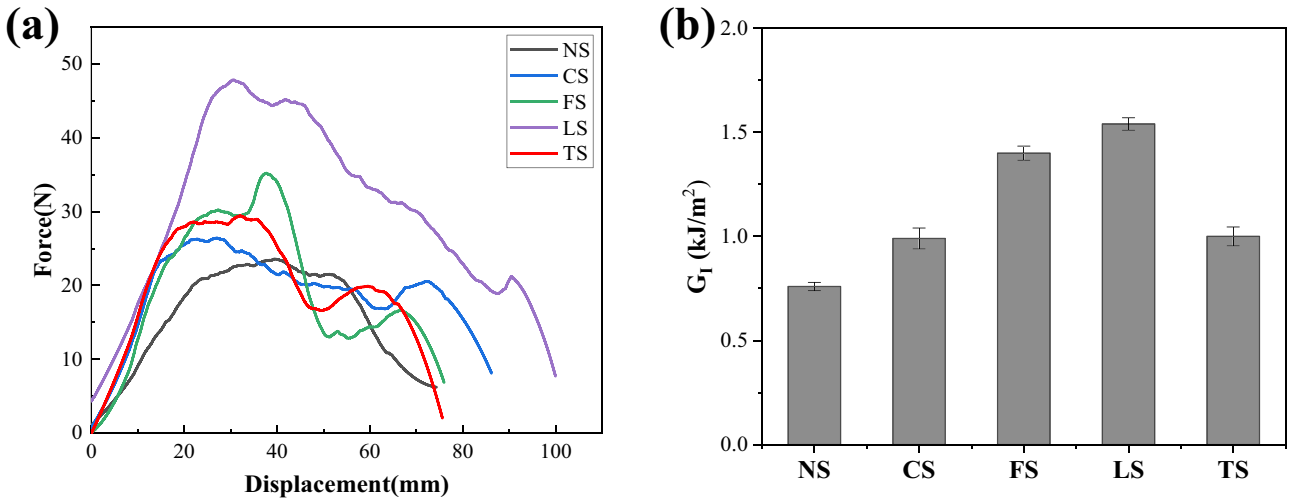

Figure 4: Comparison of various stitch methods in Mode I interlaminar test at (a) typical force–displacement curves and (b) G_I.

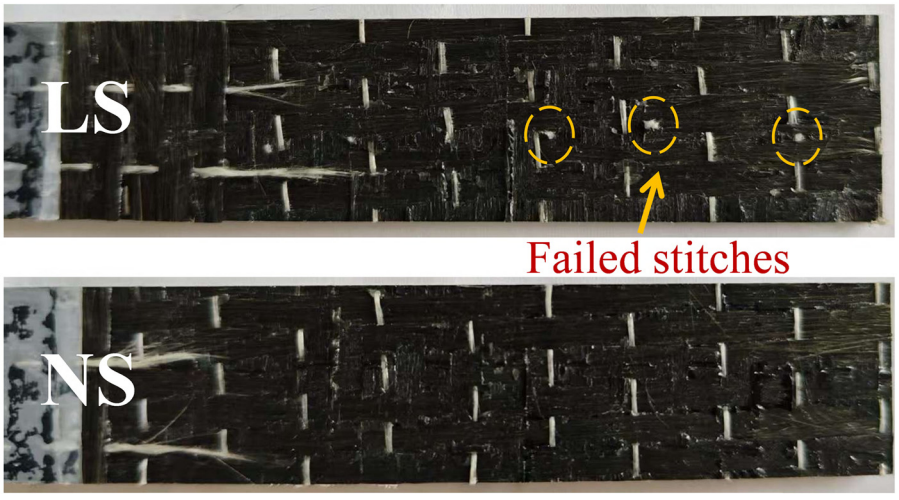

Figure 5: Failure morphology of specimens after Mode I interlaminar tests.

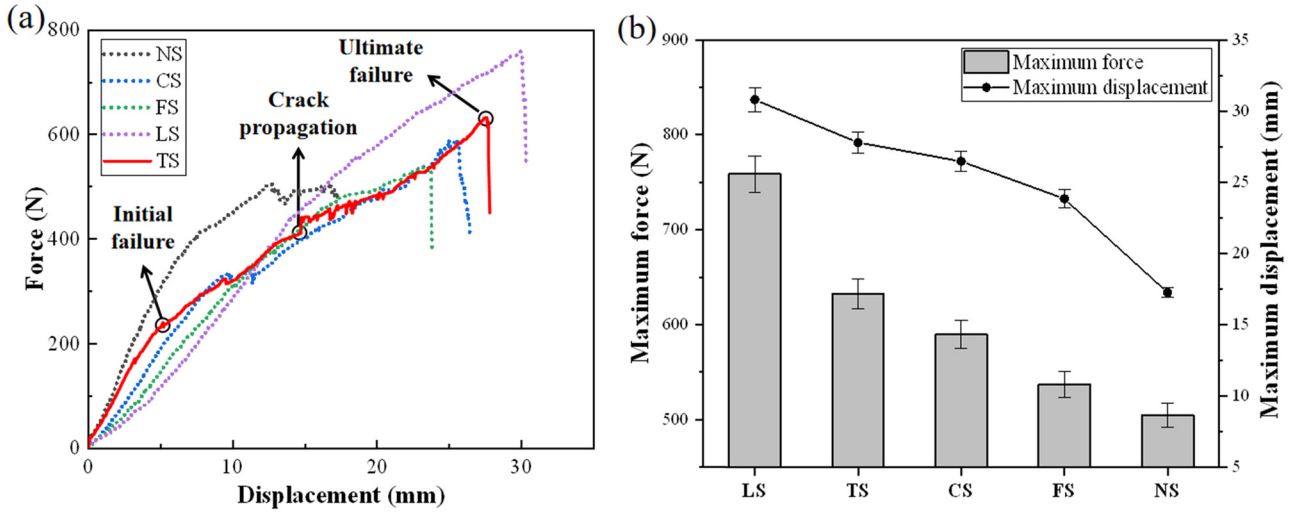

Figure 6: Comparison of various stitch methods in tension test at (a) typical force–displacement curves and (b) maximum displacement and force.

deformation stage, and the load is evenly distributed over the skin structure. As the crack increases, the vertical crack begins to propagate along the web, and the crack expands in both directions. The stitched specimen exhibits a higher ultimate force than the unstitched one, demonstrating the strength-enhancing effect of the thread. Among the stitched samples, the method of LS shows the predominant mechanical property as shown in Figure 6(b).

Damage morphology shows rapid crack growth in the triangular area of NS, CS, and TS due to weak horizontal interfaces. It can be seen from the damage morphology that the crack propagation in the triangular area of NS, CS, and TS is rapid, indicating the insufficient strength of the horizontal interface. The crack in the NS specimen propagated more toward the vertical interface than other and a unilateral fracture occurred as shown in Figure 7. This indicates that the stitching strength at the horizontal interface inhibits the propagation of horizontal cracks and enhances the tensile properties.

3.3 Effect of stitch fineness on tensile performance of T-joints

Mechanical curves in Figures 8 and 9 reveal the influence of stitch fineness on T-joint bearing performance. Under constant needle distance, the tensile load of T-joints increases as stitch fineness increases up to 1,000D. Stitch fineness exceeding 1,000D leads to a reduction in the bearing capacity of the specimen. As the fineness increases, the interlaminar failure of the T-joint becomes more obvious, which shows that the fineness of the stitch significantly affects the physical strength and failure mode. For example, the LS-1000-10 specimen achieves an ultimate load of 875.48 N, which shows an increase of 15.36% and 29.41% compared to the 500D and 1,500D specimens, respectively.

When stitch fineness is below the critical value, a moderate increase in diameter enhances mechanical anchoring and promotes a stable three-dimensional interlocking structure, thereby improving interlayer bonding while preserving carbon fiber continuity without significant damage. At this stage, the stitch–matrix interface area is appropriate to distribute load via shear stress while avoiding excessive local stress concentration. The undamaged fiber network works in tandem with the stitch so that the tensile load increases steadily with increasing fineness.

However, when the stitch fineness exceeds the critical value, the destructive effect of the stitch fineness on the structure begins to dominate. During the implantation process, the increase in the fineness of the stitch leads to a sharp increase in damage to the matrix. The originally continuous fiber force transmission paths are divided into isolated fragments, and these breaking points become fragile areas with stress concentration. Under tensile load, the cut fibers cannot share the stress, resulting in excessive concentration of the load towards the remaining fibers and threads. The microcracks around the stitch point rapidly expand under stress drive and communicate with the interface debonding area, ultimately triggering interlayer shear failure. At this time, the higher the fineness of the

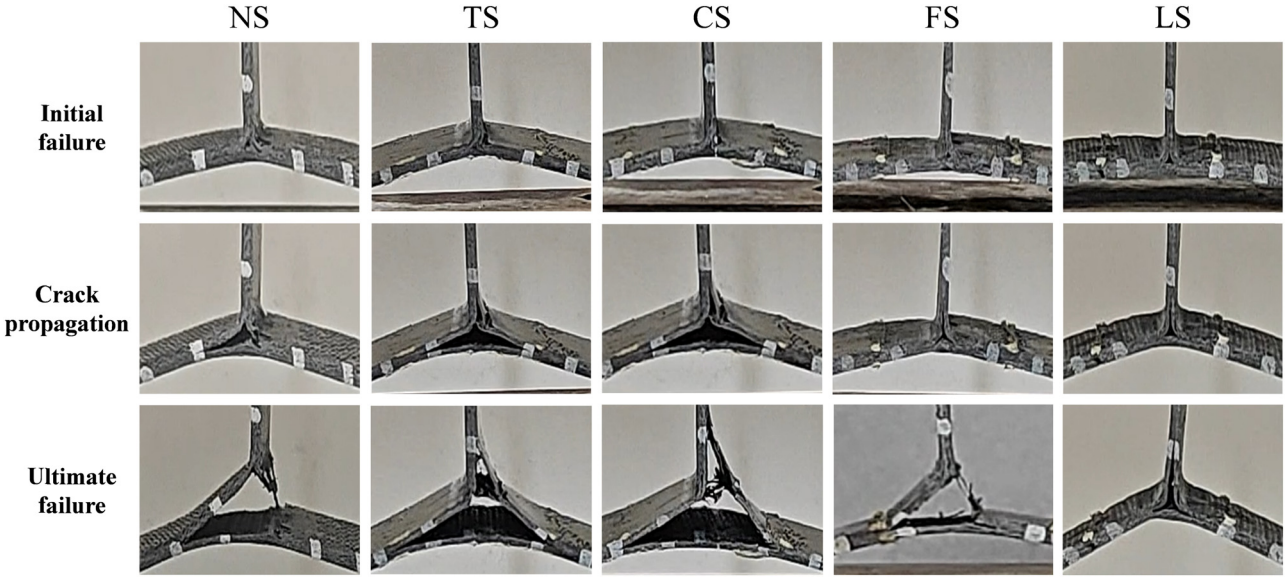

Figure 7: Tensile failure morphology of T-joints with different stitch methods under three stages.

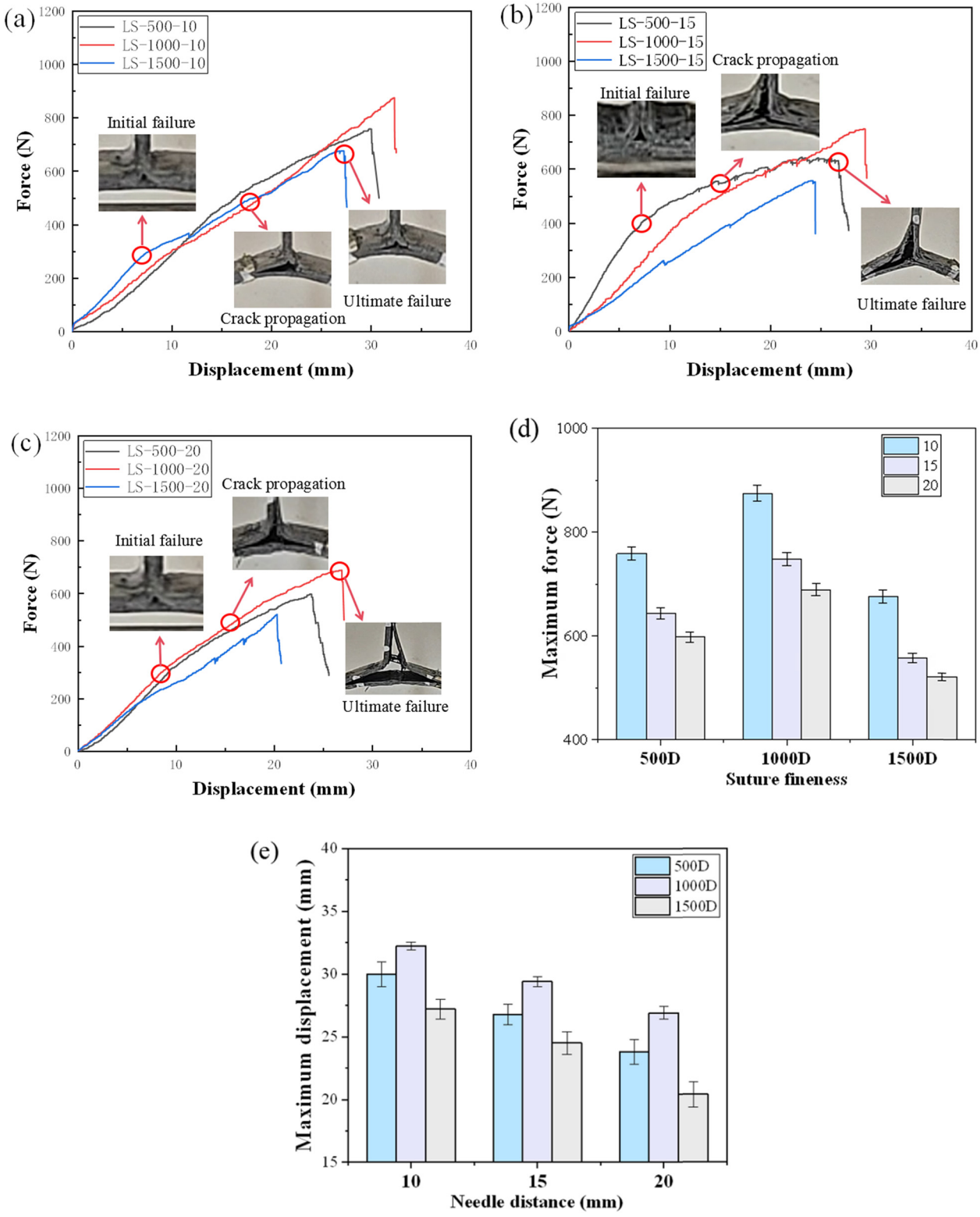

Figure 8: Comparison of various stitch fineness in tension test at (a)–(c) typical force–displacement curves and (d) and (e) their maximum displacement and force.

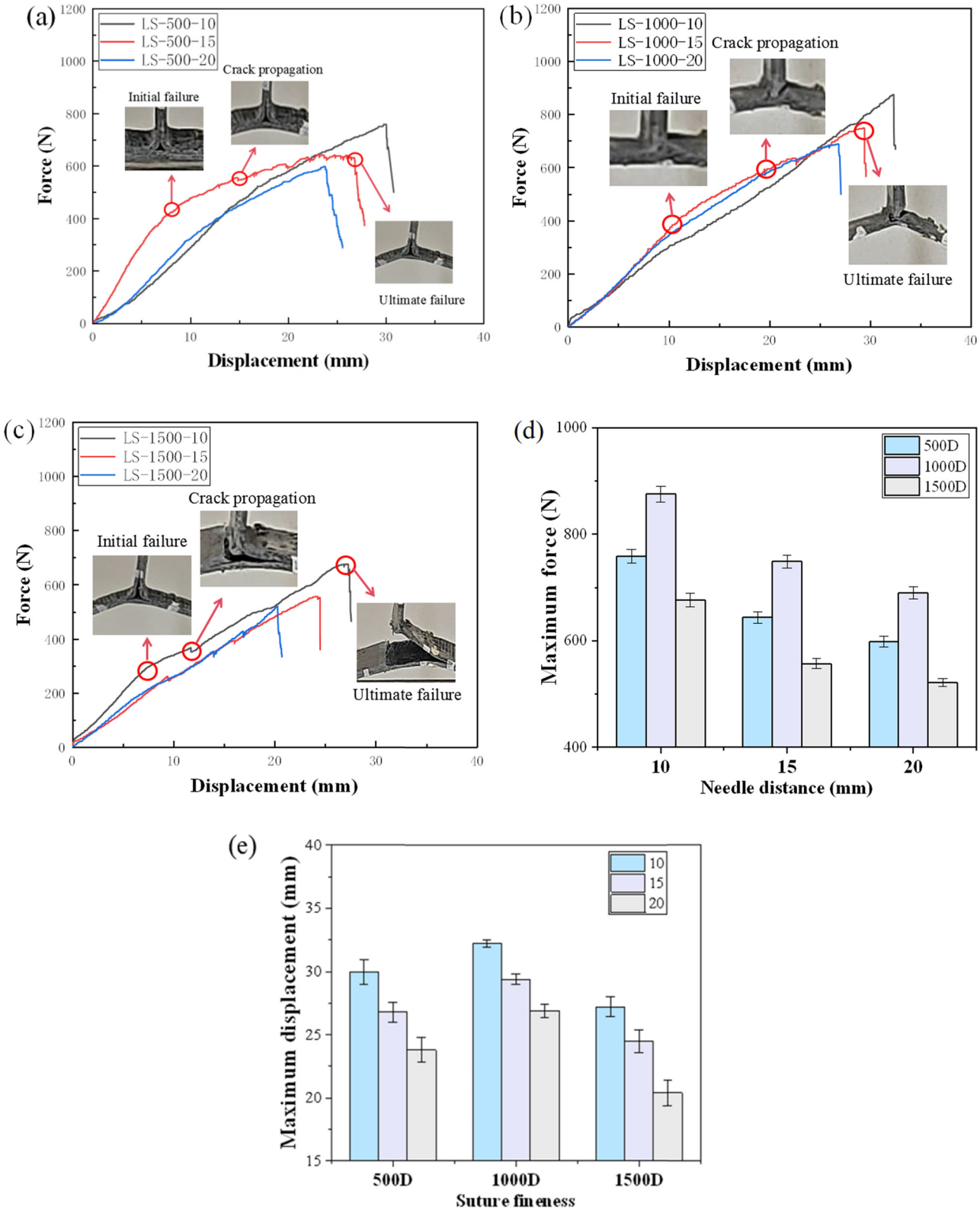

Figure 9: Comparison of various needle distance in tension test at (a)–(c) typical force–displacement curves and (d) and (e) their maximum displacement and force.

stitch, the stronger the coupling effect of fiber damage and interface failure, and the structural bearing capacity will decrease.

3.4 Effect of needle distance on tensile performance of T-joints

Stress bridging, wherein stitches span crack surfaces to transfer load and suppress opening, retards crack propagation and enhances fracture toughness. As shown in Figure 10, specimens with smaller needle distance exhibited a higher peak load. The core mechanism is attributed to an optimized failure mode governed by the enhanced network constraint effect of the denser stitches. Specifically, a reduced needle distance increases the density of mechanical anchoring points. Upon crack initiation in the triangular region, the dense network constrains the crack tip, alleviates stress concentration through interfacial shear transfer, and suppresses delamination propagation. As the crack grows, high-density stitches redistribute stress more uniformly, thereby delaying catastrophic failure.

Conversely, larger needle distance creates unreinforced regions that function as weak links. In these zones, delamination accumulates rapidly, initiating a cascade failure where adjacent stitches rupture sequentially as local stress exceeds their strength thresholds. This process culminates in the collapse of the load transfer path and a reduction in load-bearing capacity. The superior performance of specimens with smaller needle distance results from the combined effects of 3D constraint, crack suppression, and load redistribution, which maintain structural integrity and enhance peak load.

Experimental data indicate that for specimens such as the LS-500-10D, increasing needle distance from 10 to 20 mm resulted in a 22.91% reduction in ultimate load capacity, while simultaneously triggering significant exacerbation of crack propagation. This phenomenon originates from the essential function of threads in maintaining structural integrity by suppressing fiber delamination and crack advancement under tensile loading. Elevated needle distance induces non-uniform stress distribution among stitches, thereby weakening localized constraint effectiveness on fiber layers. Particularly in stress-concentrated regions like the deltoid zone, the accumulation of interlaminar shear stresses preferentially initiates delamination, subsequently promoting fiber fracture and crack propagation. Furthermore, the reduced stitch density compromises continuity in load transfer pathways, ultimately manifesting as diminished peak load capacity and degraded displacement ductility.

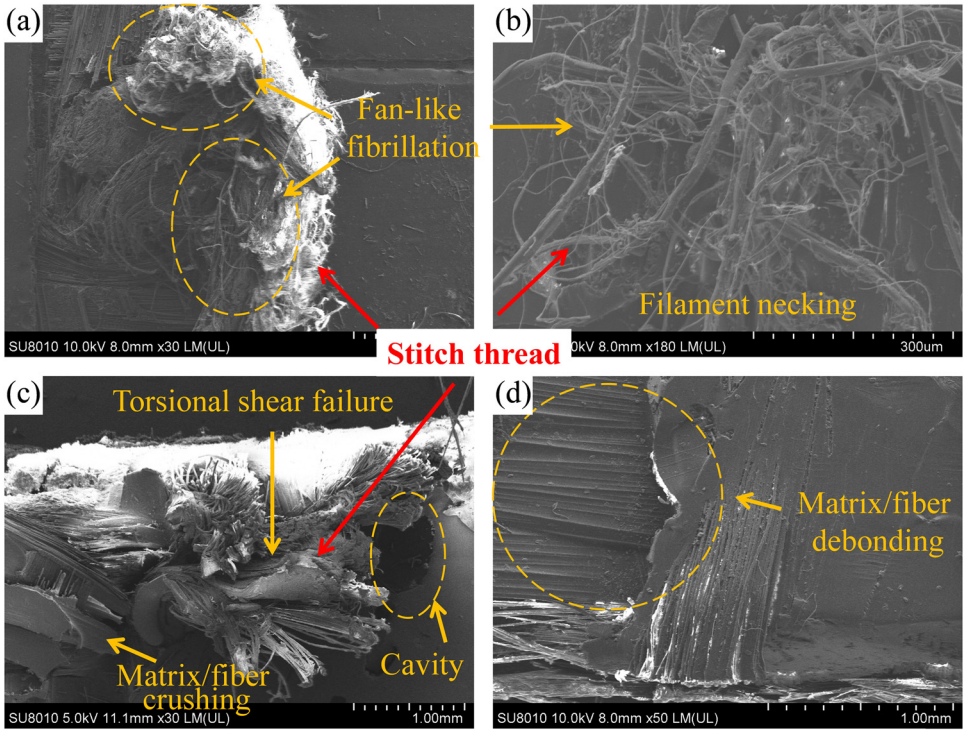

Figure 10: SEM results of stitched T-joints.

3.5 Damage mechanism of stitching enforcement

The SEM analysis established a clear relationship between the observed damage phenomena and the underlying failure mechanisms. First, the failed Kevlar threads displayed significant filament necking and fan-like fibrillation (Figure 10a–c). This ductile behavior is identified as a primary energy-dissipating and toughening mechanism. Furthermore, severe localized damage was observed around the stitch thread, including matrix/fiber crushing, matrix cavity, and torsional shear failure of the thread itself (Figure 10c). This damage is attributed to stress concentration and bridging effects of the stitch, which provide another significant mode of energy absorption. Finally, extensive fiber/matrix debonding was the dominant failure feature in the unstitched regions (Figure 10d). This observation confirms that without direct reinforcement, the inherently weak interlaminar interface dictates the final crack path, resulting in catastrophic structural failure.

Stress bridging refers to the mechanism in which reinforcement elements spanning the crack surfaces carry part of the applied load and restrain crack opening, thereby retarding crack propagation and enhancing fracture toughness.

4 Conclusion

This work focusing on key stitching parameters (stitch method, stitch fineness, and needle distance) presents a detailed experimental investigation into the tensile behavior and underlying reinforcement mechanisms of the stitched specimens. The main findings are as follows:

(1) Stitching significantly enhances the Mode I interlaminar fracture toughness and tensile load-bearing capacity of T-joints, with the improved lock stitch providing the most pronounced gains.
(2) An optimal stitch fineness (1,000D) exists, as excessive fineness degraded performance from its peak, while still outperforming the unstitched baseline. The effect arises from enhanced interlaminar constraint and more uniform stress distribution provided by stitching, while coarseness threads result in stress concentrations.
(3) Needle distance governs tensile performance, with shorter spacing enhancing constraint density and suppressing crack initiation and growth. When the needle spacing was reduced from 20 to 10 mm, the peak load increased by 27%, indicating that larger spacing weakens crack constraint and impairs tensile performance.
(4) The interlaminar toughness is primarily attributed to two significant energy absorption mechanisms: the ductile fracture of the Kevlar fibers and the stress bridging effect within the stitched regions.

Our work revealed the tension damage mechanisms of T-joints and Mode I interlaminar fracture toughness under various stitching parameters, while we also acknowledge limitations. Mode II tests reveal shear-driven crack behavior, while mixed-mode tests simulate complex service stresses, both of which are crucial for comprehensive fracture evaluation and material design. Future work will employ these tests to systematically investigate stitching reinforcement.

Funding information: This work was sponsored by the Central Government Guides Local Foundations for Science and Technology Development (Free exploration of basic research 246Z1206G).

Author contributions: Xin Jin: Project administration and methodology; Jifeng Zhang, Zhenyang Yu and Haotian Guo: Experimentation; Cuilong Liu and Xuan Gao: Data curation; Xiao Luo: Writing; Shiyao Qi: Visualization.

Conflict of interest: The authors state no conflict of interest.

Data availability statement: The datasets generated or analyzed during the current study are available from the corresponding author on reasonable request.

References

(1) Liu R, Chen J, Gong Z, Gong Z, Sun L, Dai S, et al. Enhanced mechanical performance of carbon fiber reinforced polymer composites by interface modification with self-assembled γ-Al_2O_3 nanosheet/graphene. Polym Compos. 2024;45(16):14608–19.
(2) Yang G, Zhang Q, Shi B, An T, He M, Lui Y. Application and molding procedure progress of carbon fiber reinforced polymer materials in automotive parts. Chin Plast Ind. 2023;51(11):27–33.
(3) Arhant M, Briançon C, Burtin C, Davies P. Carbon/polyamide 6 thermoplastic composite cylinders for deep sea applications. Compos Struct. 2019;212:535–46.
(4) Xue J, Wu F, Zeng C, Fan J, Guo X, Liu R, et al. Inter-tow toughness modification of carbon fiber reinforced cyanate resin matrix composites. Polym Compos. 2025;46(5):4547–57.
(5) You P, Liu C, Yao X, Xu K, Li M, Wu Y, et al. Experimental investigation on low-velocity-impact and post-impact-tension behaviors of GFRP T-joints after hydrothermal aging. e-Polymers. 2024;24(1):20240092.

(6) Chen H, Li M, Shen Z, Zhang Y, Zhu Y, Wu Y. Experimental investigation on tensile behavior of CFRP bolted joints subjected to hydrothermal aging. e-Polymers. 2024;24(1):20230183.
(7) Senol H, Ulus H, Al-Nadhari A, Topal S, Yildiz M. Ameliorating tensile and fracture performance of carbon fiber-epoxy composites via atmospheric plasma activation: Insights into damage modes through in-situ acoustic emission inspection. Compos Part A: Appl Sci Manuf. 2025;195:108929.
(8) Barzegar M, Moallem MD, Mokhtari M. Progressive damage analysis of an adhesively bonded composite T-joint under bending, considering micro-scale effects of fiber volume fraction of adherends. Compos Struct. 2021;258:113374.
(9) Hou W, Xu X, Sang L, Tong L. Failure of single hat-shaped thin-walled tubular composite T-joints under impact loading. Thin-Walled Struct. 2020;154:106815.
(10) Wu Y, You P, Li M, Xiong J, Wan Y. An experimental study on the failure mechanism of local-strengthening glass fiber reinforced polymer T-joints under/after the low-velocity impact. J Compos Mater. 2023;57(30):4699–708.
(11) Bian X, Li G, Zhang F, Zhao N. Numerical simulation study on delamination damage of composite T-joint under fatigue load. Ship Sci Technol. 2022;44(21):14–20.
(12) Xiang Y, Zhang Z, Yang X, Lin Y, Zhang G, Song C, et al. Effect of stitch density on the damage inhibition and compression strength after high-velocity impact of UHMWPE fiber composites. Compos Struct. 2024;328:117728.
(13) Mohammadi M, Sosa ME. Enhancing mode-II delamination resistance of hybrid woven composite materials of glass/Kevlar fabrics by stitching with Kevlar threads. Compos Struct. 2024;345, 118365.
(14) Ravindran AR, Ladani RB, Wang CH, Mouritz AP. Design considerations in the strengthening of composite lap joints using metal z-pins. Compos Part A. 2022;160:107031.
(15) Li Z, Lin H, Zhang Y, Wang H, Wang H, Bi Y. A novel numerical modeling procedure for investigating effect mechanism of Z-pin twist on interlayer properties of composite laminates. Thin-Walled Struct. 2025;213:113271.
(16) Fu Y, Zhu W, Li S, Li M, Xiao J, Yan L, et al. The influence of void and fractured fiber defects on the ultrafine Z-pin and Mode I fracture toughness of CFRP laminates. Compos Struct. 2025;366;119243.
(17) Tang S, Fu K, Li Y. An improved progressive damage model for three-dimensional five-directional braided composites under longitudinal compression. Compos Part A. 2025;194:108880.
(18) Su H, Han Z, Wei T, An D, Qin Q, Wei Z. Tensile mechanical properties and failure behavior analysis of three-dimensional woven composite with different apertures and braiding angles. Coat. 2025;15(4):440.
(19) Kanazawa S, Ikarashi Y, Ogasawara T, Fukuhara S, Kubushiro K, Aoki T, et al. High-temperature subcritical crack growth in a 3D woven SiC-based composite. J Am Ceram Soc. 2025;108(5):e20320.
(20) Gong B, Ouyang W, Nartey M, Wang H, Potter KD, Peng H. Minimizing the in-plane damage of Z-pinned composite laminates via a pre-hole pin insertion process. Compos Sci Technol. 2020;200:108413.
(21) Tang S, Lemanski S, Zhang X, Ayre D. Fatigue life prediction of z-fibre pinned composite laminate under mode I loading. Compos Sci Technol. 2019;174:221–31.
(22) Huang T, Wang Y, Wang G. Review of the mechanical properties of a 3D woven composite and its applications. Polym-Plast Technol. 2018;57(8):740–56.
(23) Al-Nadhari A, Ulus H, Topal S, Yildiz M. Analyzing stiffness variations in 3D woven composites: A multi-instrumental study on Glass/Kevlar hybridization effects under tensile and shear loads. Compos Part A: Appl Sci Manuf. 2025;191:108722.
(24) Ravandi M, Teo WS, Tran LQN, Yong MS, Tay TE. The effects of through-the-thickness stitching on the Mode I interlaminar fracture toughness of flax/epoxy composite laminates. Mater Des. 2016;109:659–69.
(25) Tapullima J, Kim CH, Choi JH. Analysis and experiment on DCB specimen using I-fiber stitching process. Compos Struct. 2019;220:521–8.
(26) Su X, Chen X, Zheng H, Wu K, Xin S, Guo D. Mode II interlaminar mechanical behavior of needled/stitched multiscale interlocking composites. Acta Mater Compos Sin. 2024;41(03):1567–76.
(27) Kumari S, Sinha PK. Effects of transverse stitching and hygrothermal environment on composite wing T-joints. J Reinf Plast Compos. 2003;22(18):1705–28.
(28) Zhang H, He R, Hou B, Li Y, Cui H, Yang W. Artificial hail ice impact damage of laminated composite T-joint with stitching reinforcement. Compos Struct. 2021;278:114714.
(29) Kim CH, Jo DH, Choi JH. Failure strength of composite T-joints prepared using a new 1-thread stitching process. Compos Struct. 2017;178:225–31.
(30) Bigaud J, Aboura Z, Martins AT, Verger S. Analysis of the mechanical behavior of composite T-joints reinforced by one side stitching. Compos Struct. 2018;184:249–55.
(31) Huan H, Wen L, Xiao J, Feng Q. Research on tensile properties of T-stiffened composite panels reinforced by Stitching. Sci Eng Compos Mater. 2020;(3):90–7.
(32) ASTM. (2013). Standard test method for Mode I interlaminar fracture toughness of unidirectional fiber-reinforced polymer matrix composites. ASTM D5528-13. West Conshohocken, PA: ASTM International.